Progress In Electromagnetics Research Letters, Vol. 131, 18–25, 2026

PIER Letters

(Received 2 April 2026, Accepted 20 May 2026, Scheduled 6 July 2026)

A High-Reliability Fiber-Optic Transmission System with Hybrid Power Supply

Lichao Zhang, Zheng Sun, Qi Zhang*, and Lihua Shi

National Key Laboratory on Electromagnetic Environmental Effects and Electro-Optical Engineering
Army Engineering University of PLA, Nanjing, China

ABSTRACT: Conventional fiber-optic measurement systems for pulsed electromagnetic fields are limited by power-supply instability due to the temperature sensitivity of photocells. To address this issue, we developed a highly reliable broadband fiber-optic transmission system featuring a hybrid power supply. In our design, a lithium battery serves as the primary power source for the optical transmitter, while a compact photocell provides short-term supplemental power and simultaneously recharges the battery. An additional shunt resistor (5–50 Ω) is incorporated to optimize the system input voltage. The fabricated system exhibits a 3-dB bandwidth from 5 Hz to 122 MHz, and the optical transmitter volume has been reduced to one-fifth of that in previous designs. Ten repeated electric-field measurements yielded relative errors below 3%, demonstrating excellent repeatability. Overall, the proposed system offers stable operation, low power consumption, a wide dynamic range, and strong anti-interference capability, making it well-suited for harsh electromagnetic environments.

1. INTRODUCTION

In studies of the effects of electromagnetic pulses on microelectronic systems, accurate electromagnetic-field measurements are critical. However, conventional electrical measurement systems are highly susceptible to interference from strong electromagnetic fields, which can lead to significant signal distortion. For instance, in artificially triggered lightning experiments, the return stroke current can reach tens of kiloamperes, whereas the electric field in the immediate vicinity can be as high as several hundred kilovolts per meter [1]. Measuring optical, electrical, and magnetic signals within a few tens of meters of the lightning channel poses substantial challenges due to the severe operating conditions and associated risks, which impose stringent requirements on the sensor power supply, reliability, and electromagnetic immunity.

Currently, analog fiber-optic transmission devices are widely used to transmit signals from sensors in high-intensity electromagnetic environments, with batteries serving as power sources for front-end measurement units [2, 3]. Conventional small built-in batteries often lack sufficient capacity to support prolonged experimental operation. Although all-fiber electromagnetic pulse measurement systems based on fiber-optic sensing have been extensively reported, their application in outdoor environments, such as triggered lightning experiments, is limited because of their sensitivity to ambient temperature and mechanical vibration [4, 5].

Compared with alternative power supply methods, fiber-optic power supply technology offers a safe and reliable means of energy delivery. In this approach, a laser transmits energy via a power-delivery fiber to a photocell in the front-end system of a vehicle. This technique is well-suited for long-duration, low-power continuous power supplies under harsh electromagnetic and weather conditions and has been applied in areas such as power line monitoring, the Internet of Things, and sensor powering [6, 7]. Although relatively high power levels have been demonstrated in experimental studies [8], the performance degradation caused by the temperature increase in the photocell during operation remains a critical issue affecting the stability of downstream circuits. In [9], a low-power photocell was used to directly supply power, but the resulting increase in photocell temperature adversely affected sensor performance. To address this, [10] introduced a temperature-monitoring circuit and battery-switching mechanism to prevent prolonged photocell operation under overheating conditions. However, this approach consumes a substantial portion of energy in monitoring and control circuits, increasing the required power capacity of the photocell and resulting in a bulky system with limited operational convenience.

To overcome these limitations, this study presents a highly reliable, broadband fiber-optic transmission system incorporating a hybrid power-supply architecture. The system uses a lithium battery with a relatively stable output as its primary power source. When the battery charge becomes low, a laser is activated, allowing the photocell to provide short-term power to the system while simultaneously recharging the lithium battery. The laser was deactivated once the battery was fully charged. This design reduces the demands on the photocell output stability and alleviates temperature-related effects, eliminating the need for additional temperature monitoring and regulation circuits. Consequently, a photocell with lower power requirements and a more compact form factor can be used. Measurements indicated that with a 5 W photocell, the lithium battery

* Corresponding author: Qi Zhang (emczhq@163.com).

doi:10.2528/PIERL26040203

Published by THE ELECTROMAGNETIC ACADEMY

TABLE 1. Comparison of the proposed system with existing fiber-optic transmission systems.

Feature	Ref. [9]	Ref. [10]	This study
Power supply	Single photocell	Hybrid (complex)	Hybrid (simple)
System power	1–2 W	4.5 W	1.5 W
Photocell power	5 W	15 W	5 W
Operation	Laser on/off	Computer-dependent	Laser on/off
Long-term suitability	No	Yes	Yes

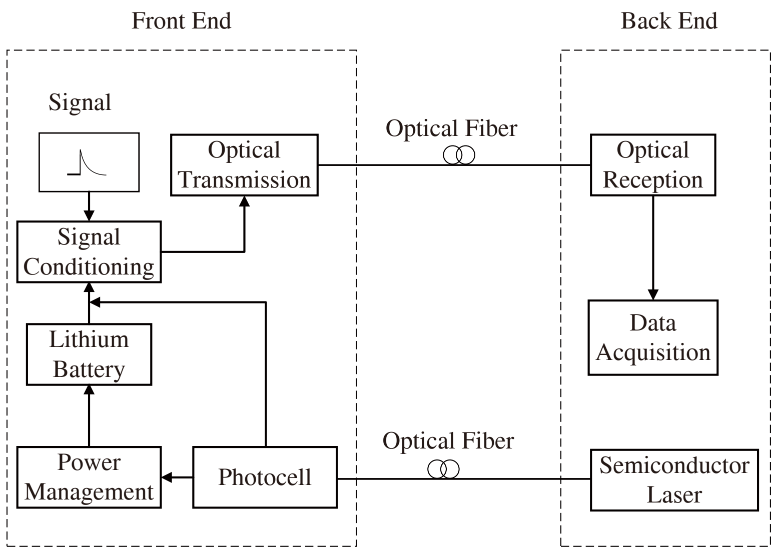

FIGURE 1. Block diagram of the overall system configuration.

charging power could reach 3 W. The optical transmitter measures 8.5 cm × 5 cm × 4 cm, occupying less than one-fifth the volume of the optical transmitter used in [10]. The proposed system retains the inherent advantages of fiber-optic technology, including a strong anti-interference capability and wide bandwidth, while offering a simplified structure, compact design, and significantly enhanced long-term operational reliability.

A comparison of the proposed system with other representative studies (Refs. [9] and [10]) is presented in Table 1.

2. SYSTEM DESIGN

2.1. System Configuration

The overall architecture of the proposed hybrid-power-supply fiber-optic transmission system is shown in Figure 1. In the front-end optical transmitter, the signal-conditioning module serves as the core unit for electro-optical signal conversion. Therefore, a power supply module based on a hybrid lithium battery and photocell architecture was incorporated. A single-cell lithium battery acts as the main power source, and its output voltage is boosted and regulated before being supplied to the signal conditioning module. A high-power gallium arsenide (GaAs) photocell converts laser light into electrical energy to supplement the lithium battery, enabling interference-free energy transmission over optical fibers. In addition, the power management module regulates the charging mode according to the lithium battery voltage to prevent adverse effects on battery performance. The back-end optical receiver converts the received optical signal into a voltage signal within the ±1 V range for output to an oscilloscope.

The proposed hybrid-power-supply fiber-optic transmission system is specifically designed for pulsed electromagnetic-field measurements under complex electromagnetic conditions, achieving the stable transmission of both signals and power.

2.2. Electro-Optical Conversion and Signal Conditioning

The electro-optical conversion module converts the voltage signal measured by the sensor into an optical signal for transmission to an optical receiver. The front-end amplification and driving circuit, which is centered around an N-channel field-effect transistor (FET), is shown in Figure 2. The measured signal is amplified and compensated; after the FET corrects the nonlinearity of optical emitter F1, the signal is converted into an optical signal using amplitude modulation. Under stable operating conditions, the total power consumption of this module was measured to be 1.5 W, representing the power drawn from the lithium battery by the module.

When measuring pulsed electromagnetic fields, the input voltage U_S of the system can easily exceed the linear input range of the subsequent driving circuit, potentially causing signal saturation distortion or even circuit malfunction. To en-

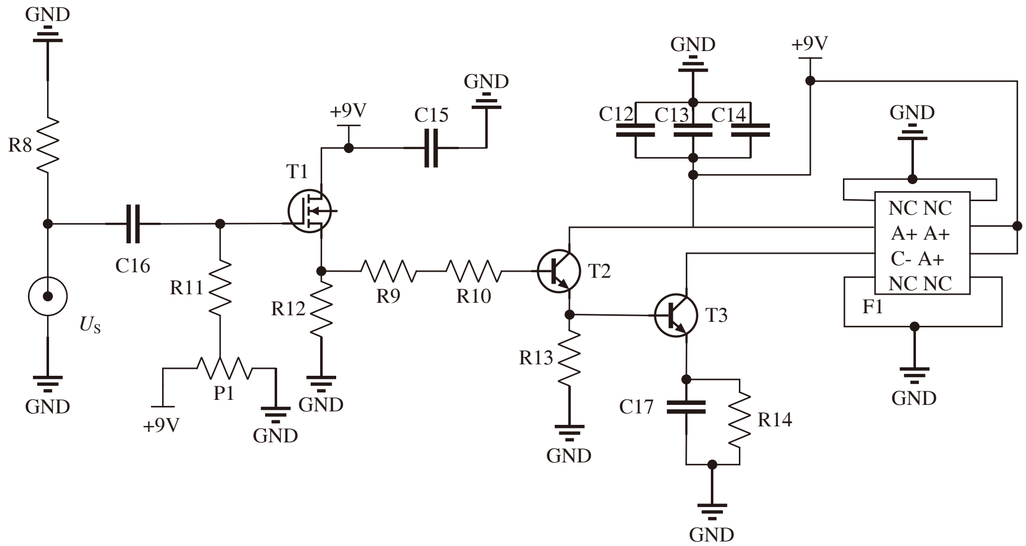

FIGURE 2. Signal conditioning and electro-optical conversion circuit.

hance the adaptability of the system to high-amplitude input signals, this study proposes an optimization scheme based on the current distribution. By introducing a shunt resistor R_1, the current distribution characteristics of the system are reconfigured.

The circuit in Figure 2 can be viewed as consisting of two parallel branches: the shunt resistor R_1 and the electro-optical conversion branch. The equivalent resistance of the electro-optical conversion branch is denoted as R_{eq}. The total current I_S at the system input node adheres to Kirchhoff's current law:

$$I_S = I_R + I_{\text{eq}} \tag{1}$$

where I_R is the current flowing through the shunt resistor, and I_{eq} is the effective operating current flowing through the electro-optical conversion branch. According to the current division principle for parallel circuits, the distribution ratio of the currents in the two branches is:

$$\frac{I_R}{I_{\text{eq}}} = \frac{R_{\text{eq}}}{R_1} \tag{2}$$

The actual current obtained by the electro-optical conversion branch is:

$$I_{\text{eq}} = \frac{R_1}{R_1 + R_{\text{eq}}} I_S \tag{3}$$

The distance from the sensor to the optical transmitter is extremely short (on the order of centimeters). For signals with rise times in the microsecond and nanosecond ranges, the wavelength λ is significantly larger than the lead length. Therefore, the transmission line effects can be neglected, and the circuit can be considered a lumped parameter system. Consequently, the shunt resistor does not affect the transmission characteristics of the system. Measurements show that with a shunt resistor of 10 Ω, the maximum input voltage of the conversion module can reach 10 V. However, the input of the optical transmitter exhibits parasitic capacitance. To optimize the system input voltage in the measured signal, it is recommended to adjust R_1 within the range of 5–50 Ω in practical implementations. Under these conditions, the sensitivity coefficient k of the fiber-optic transmission system is defined by the relationship $U_o = kU_i$, where U_i is the input voltage of the optical transmitter, U_o the output voltage of the optical receiver, and $k = 0.1$. Once a specific sensor is connected to the input of the optical transmitter to form a complete measurement system, the measurement dynamic range is jointly determined by the characteristics of the sensor and the maximum allowable input voltage of the conversion module.

2.3. Collaborative Power Supply of Lithium Battery and Photocell

To ensure long-term, stable, and cable-free operation of the measurement front-end in harsh electromagnetic environments, this study designs a collaborative power supply module based on a lithium battery and photocell. Under most operating conditions, lithium batteries serve as direct power sources. When the lithium battery charge was low, the remote optical power supply laser was activated. The electrical energy generated by the photocell was then used to charge the lithium battery via the power management module, while simultaneously providing short-term power to the system, thereby maintaining a stable operation.

To investigate the temperature effect on the photocell, a simulation model was built using MATLAB/Simulink. The equivalent circuit of the photocell is shown in Figure 3, consisting of

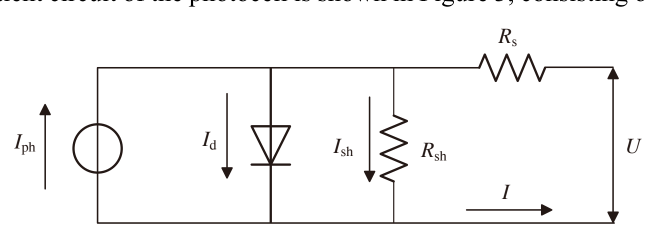

FIGURE 3. Equivalent circuit diagram of the photocell.

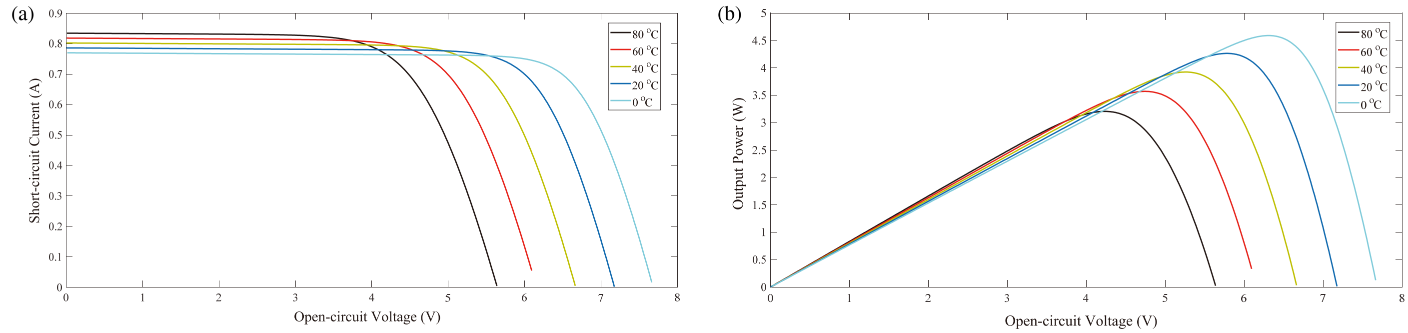

FIGURE 4. Output characteristics of the photocell under different temperatures. (a) I–V curves. (b) P–V curves.

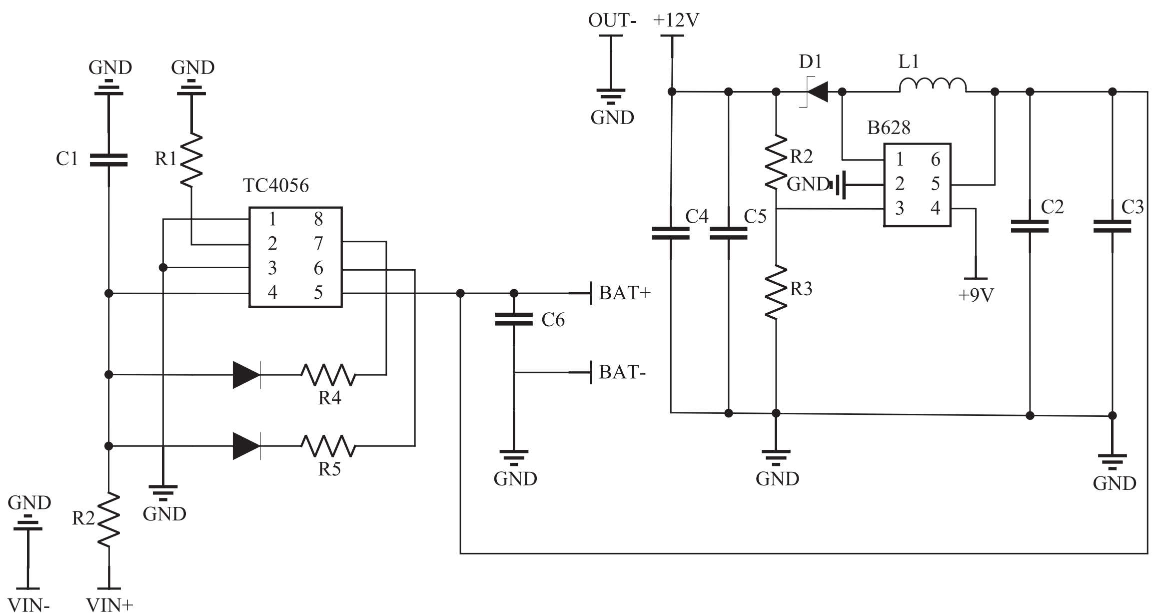

FIGURE 5. Power supply module circuit diagram.

a current source, a diode, and internal resistances (neglected in the simulation).

The irradiance (incident laser intensity) was fixed at $1\,\text{kW/m}^2$, while the temperature was varied from 20°C to 80°C in steps of 20°C. The resulting output characteristics are presented in Figure 4. As temperature increases, the output voltage drops significantly while the output current changes little, causing the maximum power point (MPP) to shift downward. This indicates that high-temperature operation severely reduces the photocell output power.

To avoid overheating and performance loss, a hybrid power supply architecture is adopted, where the photocell operates only for short durations (e.g., recharging the lithium battery). The electro-optical conversion circuit consumes 1–2 W. Considering that the actual maximum output power of a nominal 5 W photocell is typically below 5 W, a 5 W photocell was chosen to provide sufficient margin. The driving voltage of the conversion circuit requires a stable 9 V supply; hence, a B628 boost converter chip (described below) is used. Its power consumption is very low. For charge management, the TC4056A chip (with thermal pad) was selected because it offers a complete linear charging solution with reverse charging prevention, eliminating the need for an additional isolation diode.

The circuit diagram of the system's power supply module is shown in Figure 5.

This study employs a cascaded configuration of a boost converter and linear regulator to enable a single lithium battery with a nominal voltage of 3.7 V to sustain system operation. A B628 boost converter chip was selected to amplify the lithium battery voltage to 12 V. Subsequently, a linear regulator stabilizes the final output voltage supplied to the electro-optical conversion module at 9 V. The basic application circuit for the B628 boost chip is illustrated in Figure 6. This chip offers efficiency up to 95% and an input voltage range of 2–24 V. Its amplification factor is determined by external resistors R_1 and R_2, as follows:

$$V_{\text{OUT}} = V_{\text{REF}} \times \left(1 + \frac{R_1}{R_2}\right) \tag{4}$$

where the chip's feedback voltage $V_{\text{REF}} = 0.6\,\text{V}$, $R_1 = 820\,\text{k}\Omega$, and $R_2 = 43\,\text{k}\Omega$. Substituting these values yields an output voltage of approximately 12 V. The power supply path utilizing

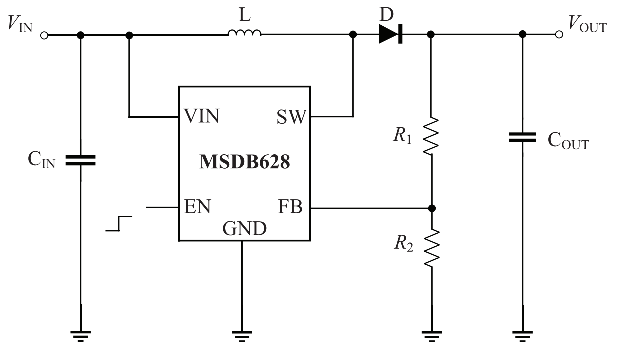

FIGURE 6. Basic application circuit of the B628 boost converter chip.

FIGURE 7. Photocell.

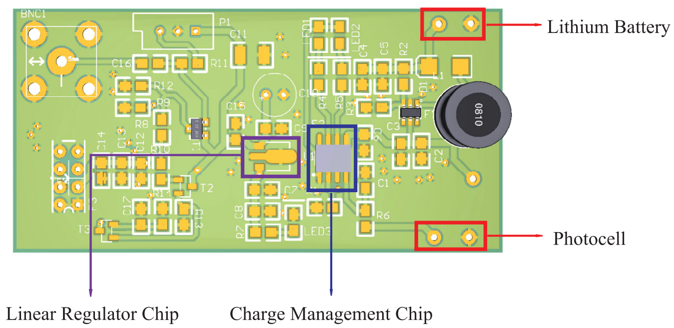

FIGURE 8. Integrated optical transmitter module.

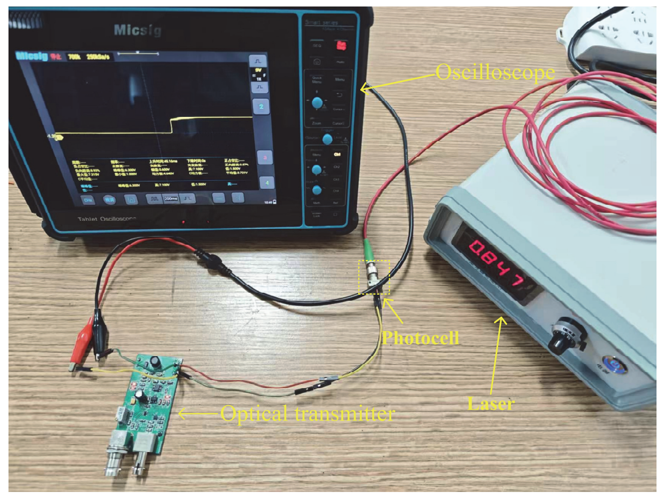

FIGURE 9. Experimental setup for system start-up time measurement.

the lithium battery, through this cascaded boost converter and linear regulator configuration, achieves both high energy efficiency and high power supply quality, providing robust support for stable system operation.

To address the challenges posed by pulsed electromagnetic-field measurement scenarios in complex environments and the limitation of battery capacity on experimental efficiency, a remote optical power supply unit was introduced. When integrated with a charge management chip, this unit enables energy supply to the system via an optical fiber.

The optical power supply unit primarily consists of a laser, photocell, and charge management chip. At the local end, a laser with an optical wavelength of 830 nm and a maximum output power of 15 W was used. A specialized single-mode fiber was used as the power transmission fiber. The charge management chip monitors the lithium battery voltage and adjusts the charging mode of the photocell for the lithium battery. As the core component supplies energy to the system during the experiments, the photocell determines the overall endurance of the sensor device. Considering the power consumption of the system and the need for portability, a compact LPC-05W-SMA-05-A photocell was selected. Its appearance is illustrated in Figure 7. Figure 8 shows an integrated optical transmitter module with dimensions of 7.5 cm $\times$ 3.5 cm.

Experimental measurements indicate that when the laser power is adjusted to achieve a $+5$ V output from the photocell, the charging power of the lithium battery can reach 3 W. As the charging time progressed, the photocell temperature increased. At a photocell surface temperature of 60°C, the photocell output voltage dropped to 4.5 V, and the charging power decreased to 2.7 W. Measurements indicate that, under normal conditions, charging a 2000 mAh lithium battery from 3 V to 4.2 V takes approximately 1.5 h. When a lithium battery was used as the sole power source, the average continuous operating time of the sensor was more than 4 h. During operation, the photocell can be operated first for 1.5 h to ensure that the lithium battery is fully charged, after which the system can be switched to lithium battery power.

3. SYSTEM RESPONSE TESTING

3.1. System Start-Up Response Time

To evaluate the activation speed of the proposed system, the start-up transient was measured. The experiment recorded the output voltage of the photocell immediately after the laser was turned on. The test setup is illustrated in Figure 9, and the measured photocell output voltage is shown in Figure 10.

As shown in Figure 10, the time from laser activation to stabilization of the photocell output voltage is approximately 0.4 s. This rapid start-up ensures that the system can be promptly energized when needed, which is particularly important for pulsed electromagnetic field measurements where timing precision is critical.

TABLE 2. Comparison of applied and measured electric fields.

No.	Applied Electric Field (kV/m)	Measured Electric Field (kV/m)	Relative Error (%)
1	0.50	0.49	2.00
2	1.00	1.00	0
3	1.50	1.48	1.33
4	2.00	2.03	1.50
5	2.50	2.51	0.40
6	3.00	2.95	1.67
7	3.50	3.57	2.00
8	4.00	4.09	2.25
9	4.50	4.42	1.78
10	5.00	5.03	0.60

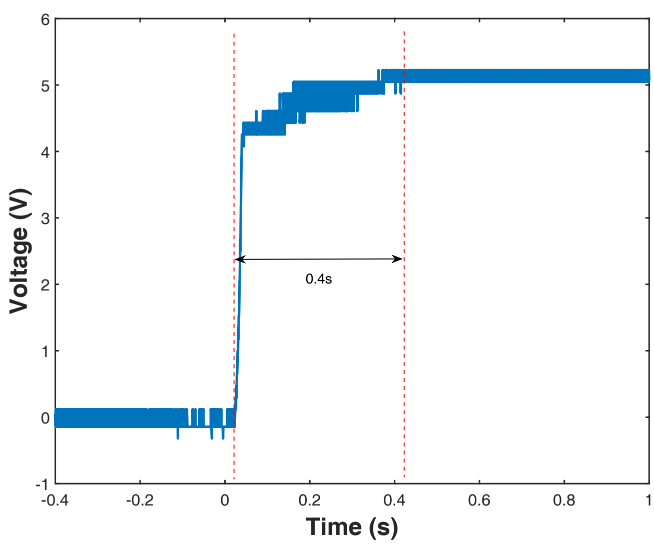

FIGURE 10. Photocell output voltage during start-up.

3.2. Pulsed Electric Field Measurement

A pulsed electric-field measurement system was constructed by connecting a monopole, electrically small antenna to the input of an optical transmitter within a fiber-optic transmission system. An electric field strength calibration system consisting of a high-voltage pulse generator and transverse electromagnetic (TEM) cell was employed. The specific experimental setup is shown in Figure 11. The high-voltage pulse generator produces a high-voltage pulse with a $1.2/50$ µs double-exponential waveform, with a maximum voltage of up to 7.5 kV. The TEM cell was used to generate a uniform, vertically polarized electric-field environment, where the electric-field strength amplitude was determined by the applied voltage divided by the separation distance (1 m).

Ten repeated tests were conducted under identical conditions to evaluate measurement consistency. Table 2 summarizes the applied electric field, measured electric field, and corresponding relative error for each test group. The results indicate that the sensor measurements closely matched the output values of the high-voltage pulse source, with the relative error remaining below 3% across all ten trials. The linearity of the measurement system is calculated to be 1.91% (full scale: 5 kV/m), demonstrating excellent linear behavior.

Figure 12 presents a set of representative normalized test waveforms. The measurement results showed a high degree of consistency between the two waveforms, indicating that the system exhibited good frequency response in both the low- and high-frequency ranges.

3.3. Pulsed Magnetic Field Measurement

A pulsed magnetic-field measurement system was established by connecting a self-integrating loop antenna, which senses the pulsed magnetic field, to the input of an optical transmitter within a fiber-optic transmission system. A strong magnetic field environment was generated using a pulsed current source and Helmholtz coil, with the specific experimental setup shown in Figure 13. The pulsed current source produced a pulse current with a $6.4/69$ µs double-exponential waveform, capable of reaching a maximum current of up to 1.5 kA. The Helmholtz coil served as the magnetic field radiator. The measurement system was placed at the center point between the two coils, where the magnetic-field uniformity was the highest, for testing. Based on the Biot-Savart law, the formula for calculating the magnetic field strength at this point is derived as follows:

$$H = \frac{NIR^2}{\left(R^2 + \left(\frac{d}{2}\right)^2\right)^{3/2}} \tag{5}$$

where N is the number of turns in each coil, I the current flowing through the coil, R the coil radius, and d the separation distance between the two coils.

Figure 14 shows the normalized test waveforms obtained from the measurement results. The two normalized waveforms exhibited good consistency in terms of rise time, pulse width, and fall time, enabling the system to perform pulsed magnetic field measurements.

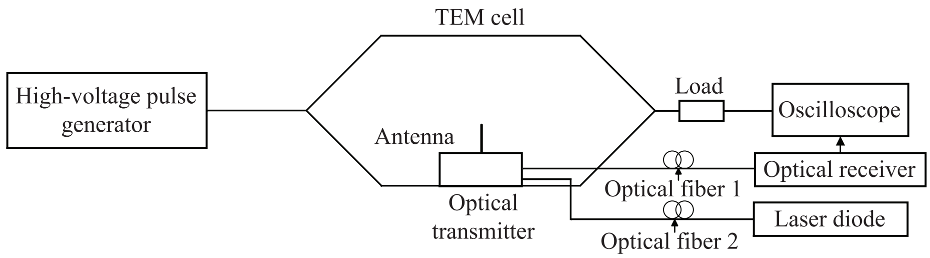

FIGURE 11. Experimental setup for electric field strength measurement.

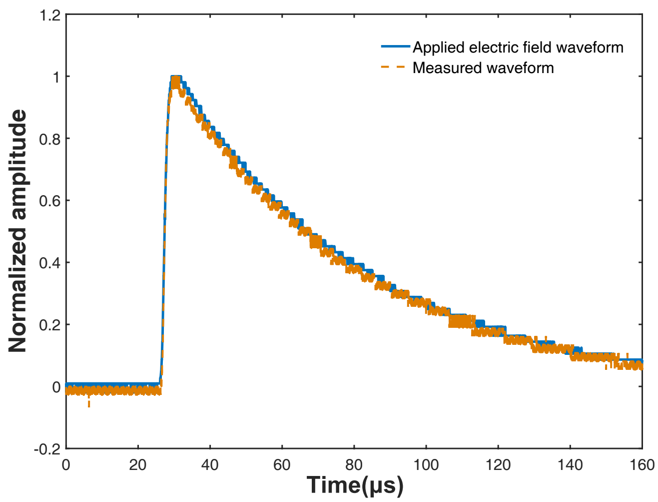

FIGURE 12. Input-output time-domain waveforms under a 1.2/50 μs excitation source.

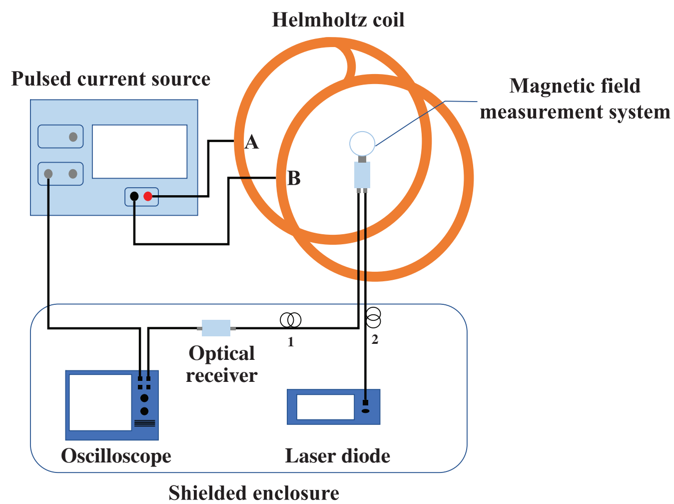

FIGURE 13. Magnetic-field intensity measurement experimental setup.

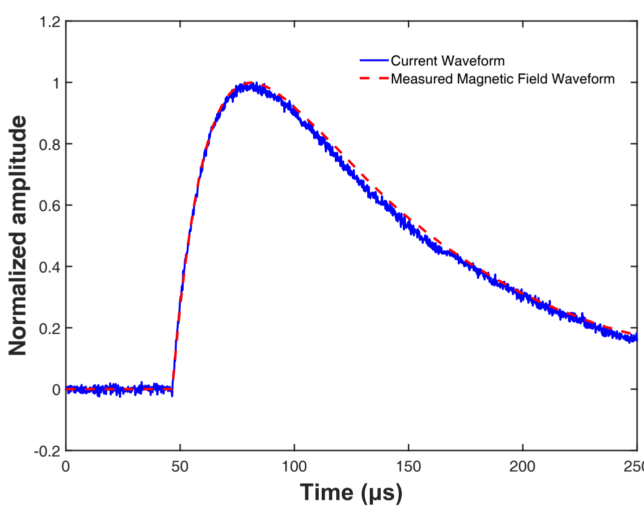

FIGURE 14. Input-output time-domain waveforms under a 6.4/69 μs excitation source.

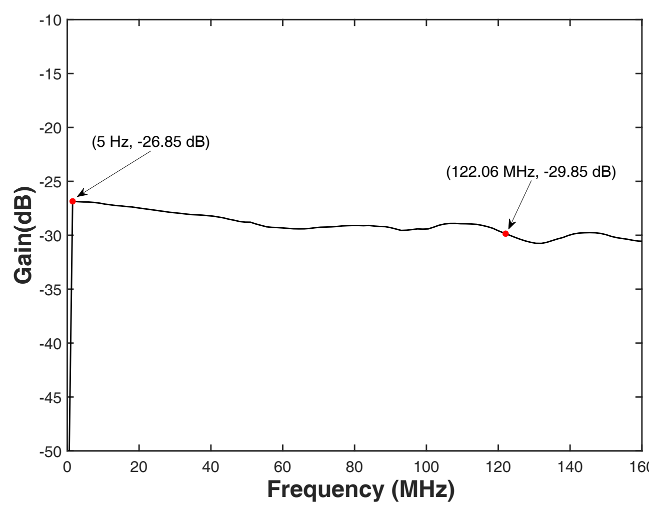

FIGURE 15. Measured frequency response characteristics of the system.

3.4. System Frequency Response Testing

Figure 15 presents the amplitude frequency response characteristics of the system measured using a network analyzer. It can be observed that the 3-dB bandwidth of the measurement system was approximately 122 MHz.

To evaluate the system's performance in capturing high-frequency signals, a high-frequency noise simulator (SKS-H04GA) was employed to inject a square wave signal with a rise time of approximately 1 ns into the system. The experimental configuration is shown in Figure 16, and the test results are presented in Figure 17. The measured waveform follows the same trend as the injected signal, but the rise time of the injected signal is about 0.8 ns while the measured rise time is about 3.1 ns. It can be inferred that the system's test bandwidth is approximately 115 MHz, which is in good agreement with the 122 MHz bandwidth measured by the network analyzer.

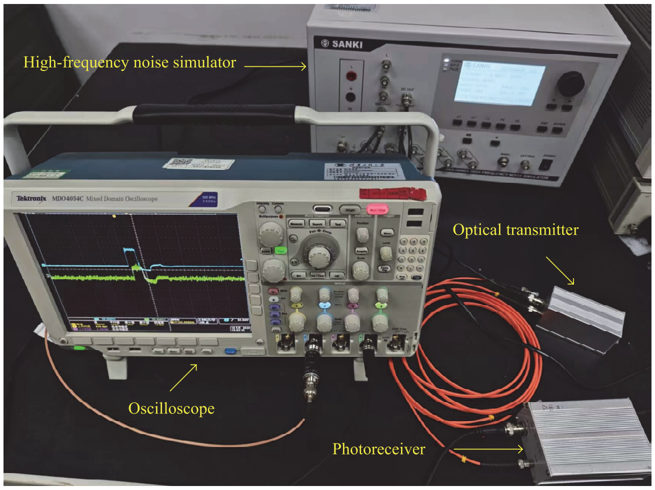

FIGURE 16. Experimental setup for square wave injection.

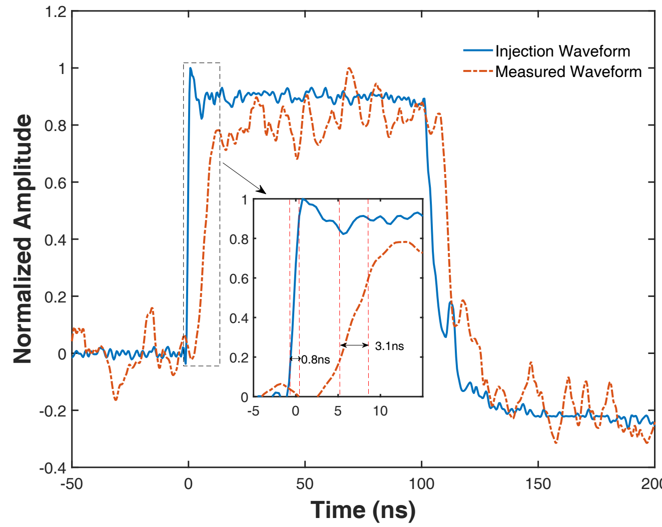

FIGURE 17. Square wave test results.

4. CONCLUSION

This study has addressed the issue of power-supply stability in fiber-optic transmission measurement systems operating in harsh electromagnetic environments by designing and implementing an improved fiber-optic transmission system based on a lithium battery buffer architecture. The proposed solution resolves the stability problems caused by elevated temperatures affecting the photocell and the overall system, while eliminating the need for additional feedback and control circuits, thereby reducing system complexity. Experimental validation demonstrates that the system is suitable for pulsed electromagnetic-field measurements in complex electromagnetic environments. Compared with other fiber-optic transmission systems employing different power supply methods, the proposed system offers advantages such as stable endurance, low power consumption, a wide dynamic range, and a strong anti-interference capability. This study provides an effective and practical solution for long-term, reliable signal monitoring in remote and complex electromagnetic environments, such as high-voltage substations and lightning electromagnetic pulse scenarios.

ACKNOWLEDGEMENT

The authors acknowledge the support of the National Key Laboratory on Electromagnetic Environmental Effects and Electro-Optical Engineering. This work was also supported by the China Key Lab Foundation under Grant No. 61422062403 and Grant No. JCKYS2025LD3.

REFERENCES

[1] Li, S., S. Qiu, and L. Shi, "Characteristics of electric field peaks and its variation rate with the distance in the near field of lightning," *Chinese Journal of Radio Science*, Vol. 34, No. 4, 531–535, 2019.

[2] Wang, W., Z. Zhu, X. Nie, J. Yang, Y. Shi, and J. Wang, "A magnetic field measurement technology of high altitude electromagnetic pulse," *Chinese Journal of Radio Science*, Vol. 34, No. 3, 347–354, 2020.

[3] Liu, Y., L. Ma, Y. Cheng, W. Wu, J. Guo, and M. Zhao, "Pulse electric field measurement system with sensitivity self-calibration based on optical fiber transmission," *High Voltage Engineering*, Vol. 47, No. 4, 1478–1484, 2021.

[4] Xu, F. H., F. J. Ding, L. Chen, L. Liu, and Y. S. Cao, "Performance analysis on integrated optical electric field sensor for high-accuracy nanosecond intense electromagnetic pulse measurement," *Semiconductor Optoelectronics*, Vol. 40, No. 6, 793–795, 2019.

[5] Sima, W., L. Zeng, M. Yang, T. Yuan, and P. Sun, "Improving the temperature and vibration robustness of fiber optic current transformer using fiber polarization rotator," *IEEE Transactions on Instrumentation and Measurement*, Vol. 71, 1–12, Jan. 2022.

[6] Yan, J., J. Wang, C. Gao, J. Jiang, Y. Lu, Z. Liu, S. Cao, and X. Jiang, "Design and realization of a power-over-fiber sensor system for internet of things," *Journal of Optoelectronics·Laser*, Vol. 26, No. 8, 1513–1519, 2015.

[7] Wang, T., H. Chen, M. Xie, Y. Lu, and J. Wang, "Design of gas sensor system based on power-over-fiber," *Chinese Journal of Sensors and Actuators*, Vol. 33, No. 10, 1516–1521, 2020.

[8] Matsuura, M., N. Tajima, H. Nomoto, and D. Kamiyama, "150-W power-over-fiber using double-clad fibers," *Journal of Lightwave Technology*, Vol. 38, No. 2, 401–408, Jan. 2020.

[9] Fu, Y.-P., C. Gao, B. Yang, Y.-X. Li, and L.-H. Shi, "Research on zifeng tower lightning current full wave measurement," *Journal of Microwaves*, Vol. 33, No. 5, 24–29, 2017.

[10] LI, Y., L. Shi, Q. Zhang, and S. Li, "Design and experiment of power over fiber electric field measurement system for lightning electromagnetic pulse," *Chinese Journal of Radio Science*, Vol. 38, No. 3, 445–452, 2023.